INVERSE HEAT CONDUCTION PROBLEM USING COMPACT FINITE DIFFERENCE SCHEME

Mohammad Javad Maghrebi

The Faculty of Mech. Eng.,
Shahrood Uni. of Tech.,
Shahrood, I. R. Iran
javad@shahrood.ac.ir

Ahad Zabett

Materials Sci. and Eng. Dept.,
Ferdowsi Uni. of Mashhad,
Mashhad, I. R. Iran
ahad@um.ac.ir

ABSTRACT

Numerical Simulation of inverse heat conduction problem is conducted in one dimensional polar coordinate system. This simulation is performed in order to properly determine the boundary condition required for a obtaining a specific form of a metal properties by heat treatment of a specimen in an oven. The determined boundary condition is then used in the direct numerical simulation of time dependent heat conduction problem to check the accuracy the inverse solution. The boundary condition which is proposed by the inverse method is found to be appropriate for producing the desired metal property. Therefore, in this study the oven desirable condition which produce a known metal properties is obtained. The conditions obtained by the inverse numerical simulation can be used in the heat treatment of a metal contained in an oven under controlled boundary conditions. This shows the unique ability of numerical modeling to determine exact applicable conditions for an oven used for the heat treatment of metals. The traditional method uses the trial and error approach which is very time consuming and cost-demanding. In the inverse simulation part of this study a prescribed and a Neumann boundary condition are imposed at the inlet boundary of the rod while in the direct simulation a prescribed boundary condition at the outlet and a null Neumann boundary condition at the inlet are imposed. The spatial derivatives are calculated using a compact finite difference scheme. Computation are advanced in time using compact third order Runge–Kutta scheme. The numerical results are followed by the discussion for the heat treatment of an alloy steel rod.

1. INTRODUCTION

A computerized method based on a phenomenological model of the kinetics of transformations taking place under non–isothermal conditions for simulating the metallurgical processes occurring during the hardening and tempering of steels was studied by Reti and Gergely [1]. The proposed program was found to be suitable for constructing new-type CCT–diagrams related to different workpiece geometries. Transformation kinetics of various phases were modeled thermodynamically by Umemoto et. al. [2]. This was performed to make quantitative prediction of microstructure in HSLA steels produced by isothermal or continuous cooling transformation. They studied five different kinds of phases namely, polygonal ferrite, Widmanstatten ferrite, pearlite, bainite and martensite, and ten alloying elements. Details of the involved transformation kinetics were studied by means of numerical simulation. The effects of work-hardening of austenite on the nucleation and growth rates of various phases were discussed and a mathematical model of transformation kinetics from work–hardened austenite was also presented. Suehiro [3] developed a mathematical model for predicting phase transformation of hypoeutectoid steels during continuous cooling. The model contains only a small number of experimental parameters so as to be used in wide ranges of temperature and chemical composition. Computer simulation of microstructural changes and the relationships between microstructure and mechanical properties of hot rolled steel products has been studied by Kwon [4]. A new technology emerged from the modeling studies, attempting to predict the microstructural changes occurring during hot rolling and cooling of steels and to control their mechanical properties so that production was carried out under the optimum processing condition. This computer aided prediction and control technology is performed by means of the mathematical models based on physical metallurgy. Kurpisz-K Nowak-AJ [5] investigated the inverse problem of the temperature and heat flux prediction on the surface of a heat conducting body. Since the problem belongs to the ill-posed, the method of solving the boundary problem as well as the method of stabilizing the results of calculations were used. The boundary element method was applied to solve the boundary problem. To obtain stable results a combined 'future steps' and regularization method were applied. A numerical example was given in the paper which ensure the stability of the results. In the current study, the inverse heat conduction problem is solved by means of numerical simulation. This is to performed to obtain a boundary condition which is under control in a real heat treatment process. The compact finite difference scheme of Lele [6] is used to calculate the spatial derivatives and a compact third order Runge–Kutta scheme of Wray [7] is used for the time advancement scheme. The results indicates that the method is quite efficient in determining a proper boundary condition for the rod surface. The obtained boundary condition is used in direct heat conduction problem to verify the results.

2. GOVERNING EQUATIONS

Time dependant heat conduction problem in one dimensional polar coordinate system is described by the following equation.

$$\frac{\partial T}{\partial t} = \frac{\alpha}{r}\frac{\partial}{\partial r}(r\frac{\partial T}{\partial r}) \qquad (1)$$

where α is thermal diffusivity. Since the boundary condition along the rod is symmetrical any change in azimuthal direction is ignored. The temperature variation in longitudinal direction is not

studied. These indicates that the computational domain is the radius of a rod under investigation. An exact condition to apply a rod placed in an oven used for the thermal treatment which produce a desirable mechanical property at the center of the rod is sought. The desirable condition corresponds to the temperature–time history which is not applicable in an oven of heat treatment. However, the condition can be imposed as a boundary condition in a numerical simulation of inverse heat conduction problem. This produce a proper boundary condition that can be applied in practice. In numerical simulation of direct heat conduction problem the obtained boundary condition is used to check the accuracy of the results. That is to verify the temperature–time history at the center of the rod used as a boundary condition in the inverse simulation.

3. INITIAL CONDITION AND BOUNDARY CONDITION OF INVERSE PROBLEM

The governing equation (Eq. 2) is first order in time and second order in space. This indicates that one initial condition and two boundary conditions are required to perform the numerical simulation. In inverse part of the simulation, which produce temperature for whole of the domain including the surface temperature of the rod, two boundary conditions are imposed at the center of the rod. They are Dirichlet and Neumann boundary conditions. The Dirichlet boundary condition pertains to the temperature–time history and the Neumann boundary condition corresponds to the rate of change of temperature are:

$$T(r=0,t) = \tau(t).$$

$$\frac{\partial T(r=0,t)}{\partial r} = 0.$$

The room temperature is used to set the initial condition of the rod. That is

$$T(r,t=0) = \psi(r).$$

4. OVEN TEMPERATURE PREDICTION

The balance of energy at the surface of the rod subjected to both radiation and convection is used to determine the oven temperature. This is the oven temperature which can be used in a real practical work. The energy balance states that:

$$\frac{\partial T(r=R,t)}{\partial r} = h(T(R,t) - T_\infty(t)) + \sigma(T^4(R,t) - T_\infty^4(t)) \tag{2}$$

where $T_\infty(t)$ is the oven temperature time history. Solution of the inverse heat conduction problem shows that all terms in Eq. 4 are known except $T_\infty(t)$. This is a polynomial of the fourth order and can be solved by the method of Bairstorw.

5. INITIAL CONDITION AND BOUNDARY CONDITION OF THE DIRECT PROBLEM

In direct part of the simulation, the accuracy of the results obtained in inverse simulation is verified. The computational domain contains the rod center while the rod surface is not included. In other words, the rod's surface temperature is taken into account as a Dirichlet type boundary condition. Due to the symmetric condition at the rod center a null Neumann boundary condition is applied as before. Therefore, the Boundary conditions are

$$T(r=R,t) = \tau_1(t)$$

$$\frac{\partial T(r=0,t)}{\partial r} = 0.$$

Temperature distribution obtained at the final stage of heat treatment is considered as initial condition in the direct simulation. That is

$$T(r,t=T) = \phi(r).$$

6. NUMERICAL MODELING OF SPATIAL DERIVATIVE

The details of the numerical methods used to solve the governing equation 2 , subject to their boundary conditions are described. The spatial derivatives are computed using the Padé (compact) finite difference scheme developed by Lele [6]. He introduced the first derivative of $T(r)$ implicitly according to

$$\alpha T_{j-1}^{'} + T_j^{'} + \alpha T_{j+1}^{'} = \frac{\alpha+2}{3\Delta r}(T_{j+1} - T_{j-1}) + \frac{4\alpha-1}{12\Delta r}(T_{j+2} - T_{j-2}), \tag{3}$$

where a prime denotes the first derivative, j represents the grid number ($0 \le j \le J$) and $\Delta r = L_r/J$. By setting $\alpha = 1/4$ or $\alpha = 1/3$ a fourth-order or sixth-order accurate scheme is obtained. At the streamwise boundaries (e.g. at $j = 0$ and $j = J$) an implicit one-sided, third-order derivative approximations is used:

$$T_0^{'} + 2T_1^{'} = \frac{1}{2\Delta r}(-5T_0 + 4T_1 + T_2), \tag{4}$$

and

$$T_J^{'} + 2T_{J-1}^{'} = \frac{1}{2\Delta r}(5T_J - 4T_{J-1} - T_{J-2}). \tag{5}$$

At the vicinity of the boundary (e.g. at $j = 1$ and $j = J-1$) the general form of the first derivatives (Eq. (3)) is used with $\alpha = 1/4$. Lele [6] discussed that replacing of α by $\alpha^{'} = (16\alpha + 32)/(40\alpha - 1)$ at $j = 2$ and $j = J-2$ guarantees the stability and numerical conservation of $(\partial/\partial t)u = (\partial/\partial r)T(u)$. This is taken into account here. Figure 1 shows the accuracy of the Padé finite difference scheme for the first derivative of $T(r) = \sum_{k=-N/2}^{k=N/2} \hat{T}(k)\exp(2\pi ikr/R) + c.c.$ where c.c. denotes a complex conjugate. The Padé finite difference scheme is an implicit scheme. It is expected to realize a

third order accurate scheme at the boundaries and a sixth order accurate scheme far from both boundaries (e.g. at $r = R/2$). Figure 2 shows the order of accuracy. The figure clearly indicates the third, fourth and the sixth order of accuracy, for the first derivative approximations using Eq. (4) at the boundaries and Eq. (3) with $\alpha = 1/3$ and $\alpha = 1/4$ at $r = R/2$ (which is far from both boundaries).

Equation (6) represents the second derivative of $T(r)$, which is a family of fourth order accurate Padé finite difference schemes.

$$\alpha T_{j-1}^{''} + T_j^{''} + \alpha T_{j+1}^{''} = \frac{4(1-\alpha)}{3\Delta r^2}(T_{j-1} - 2T_j + T_{j+1}) + \frac{10\alpha-1}{12\Delta r^2}(T_{j-2} - 2T_j + T_{j-2}). \tag{6}$$

where $\alpha = \frac{1}{4}$. At the boundaries, one–sided, third order schemes are used. They are:

$$T_0^{''} + 11T_1^{''} = \frac{1}{\Delta r^2}(13T_0 - 27T_1 + 15T_2 - T_3), \tag{7}$$

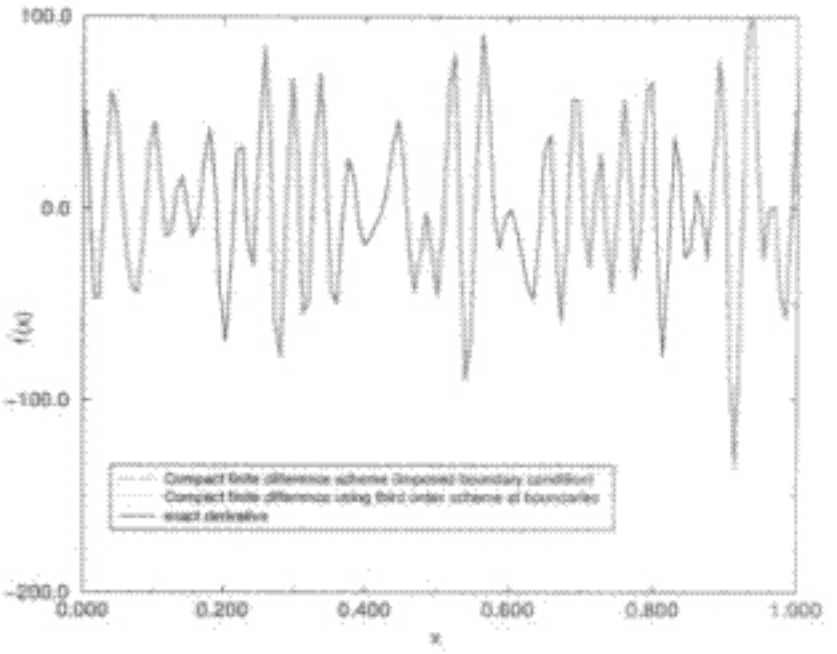

Figure 1: First derivative approximation of $T(r_j)$ using sixth order Padé finite difference scheme using $N = 64$, $R = 1.0 \leq j \leq 128$ and $T(r_j) = \sum_{k=-N/2}^{k=N/2} \hat{T}(k) \exp(2\pi i k r_j / R) + c.c.$.

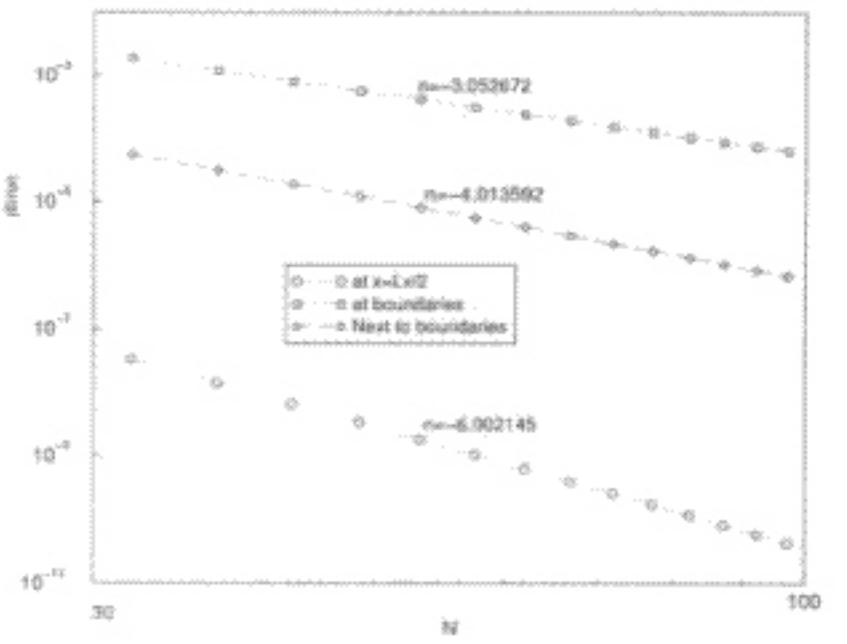

Figure 2: Order of accuracy for first derivative approximation using Padé finite difference scheme.

and

$$T_J^{''} + 11T_{J-1}^{''} = \frac{1}{\Delta r^2}(13T_J - 27T_{J-1} + 15T_{J-2} - T_{J-3}). \quad (8)$$

Taking the first order derivative from both sides of Eq. (4) gives

$$T_0^{''} + 2T_1^{''} = \frac{1}{2\Delta r}(-5T_0^{'} + 4T_1^{'} + T_2^{'}), \quad (9)$$

which simplifies to

$$T_0^{''} + 2T_1^{''} = \frac{-3}{\Delta r}T_0^{'} + \frac{1}{2\Delta r}(T_0^{'} + 4T_1^{'} + T_2^{'}). \quad (10)$$

Substituting the left–hand–side of Eq. (4) (using $\alpha = 1/4$) for the terms in the parenthesis of Eq. (10) forms the following equation.

$$T_0^{''} + 2T_1^{''} = -\frac{3}{\Delta r}\frac{dT}{dr}|_{(r=0)} - \frac{3}{2\Delta r^2}(T_0 - T_2). \quad (11)$$

Equation (11) is used at the inlet boundary of computational domain i.e. at the rod center. In the immediate vicinity of the boundaries (at $j = 1$ and $j = J - 1$), the second–order compact finite difference scheme Eq. (??) is used with $\alpha = 1/10$. Figure 3 shows the order of accuracy for the second order Padé finite difference scheme at boundaries and at $r = R/2$. It clearly indicates that the numerical scheme is third order accurate at the end boundaries, and fourth order accurate at $r = R/2$. The compact finite difference scheme is an implicit scheme, hence the highest order of accuracy can be obtained at the furthest distance from both boundaries where the lower order scheme are used.

7. TIME ADVANCEMENT SCHEME

A compact, third order, Runge–Kutta time differencing scheme developed by Wray [7] is used to advance the computation in time. Application of the time advancement scheme to the following model equation

$$du/dt = R(u) \quad (12)$$

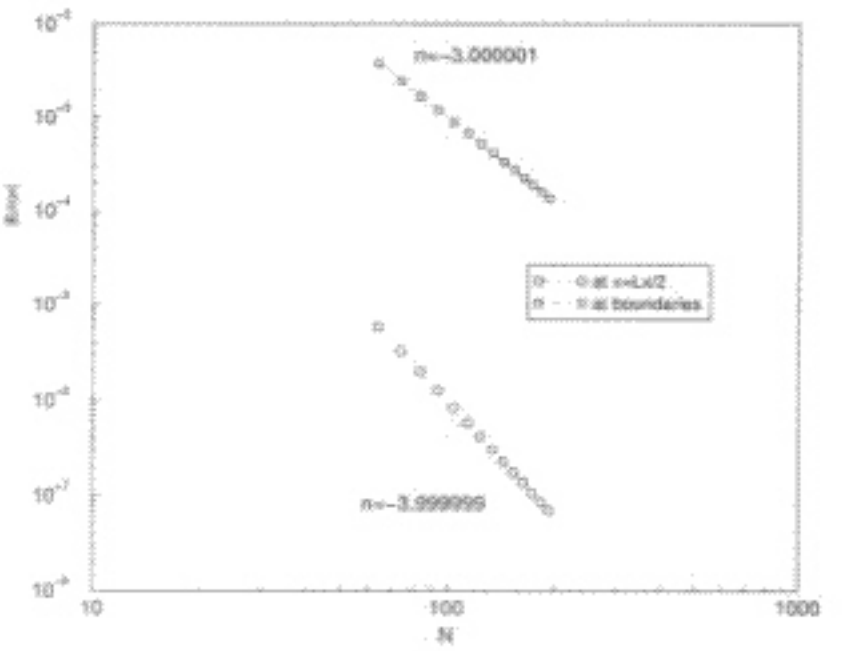

Figure 3: Order of accuracy for second derivative approximation using Padé finite difference scheme.

Time	First location	Second location
t^n	u^n	$R(u^n)$
$t^{'} = t^n + c_1\Delta t$	$u^{'} = u^n + c_1\Delta t R$	$R^{'} = R(u^{'})$
$t^{''} = t^{'} + (c_2 + d_2)\Delta t$	$u^{''} = u^{'} + (c_2 R^{'} + d_2 R)\Delta t$	$R^{''} = R(u^{''})$
$t^{n+1} = t^n + \Delta t$	$u^{n+1} = u^{''} + (c_3 R^{''} + d_3 R^{'})\Delta t$	

Table 1: Third order Runge–Kutta time advancement scheme [7].

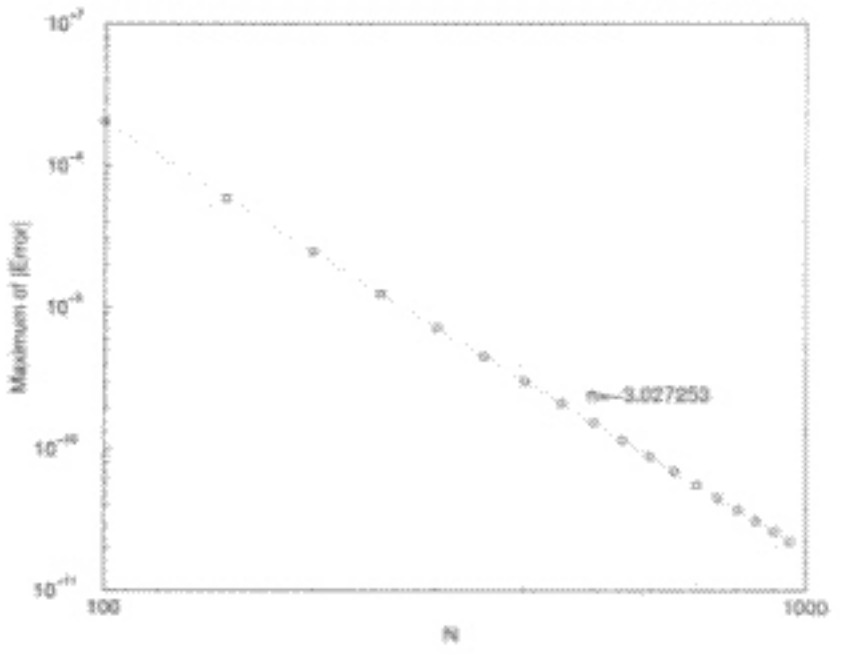

Figure 4: Order of time advancement scheme for $du/dt = -u(t)$ with $u(0) = 1$.

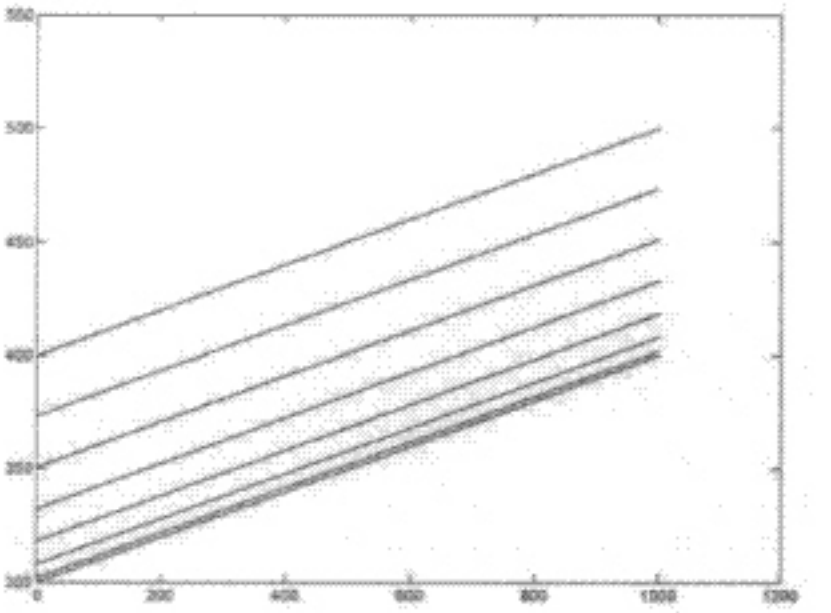

Figure 5: Temperature–time trace in both inverse and direct heat conduction simulation for the test case of $T(r,t) = 300+t+4\alpha r^2$

is performed in three sub–steps according to Table. 1.

The table shows that the time advancement of Eq. (12) by one time increment (Δt) requires computation of the right–hand side (R) in three successive sub–time–steps. In each of these sub–steps, time (t) is incremented by $(c_i + d_i)\Delta t$ and u is accumulated by linear combination of R associated with the current time level and that of the previous sub–time–step. Results in the second column of the third sub–time–step is regarded as solution incremented by Δt.

The coefficient used in the time advancement scheme (c_i, d_i) can be obtained using the Taylor series expansion for R' and R'' and equating the terms of like orders. This leads to

$$\begin{aligned} c_1 + c_2 + c_3 + d_1 + d_2 + d_3 &= 1, \\ c_1c_2 + c_3[\frac{d_2}{c_2}(1 + \frac{d_3}{c_3}) + c_2(1 + \frac{d_2}{c_2})] &= \frac{1}{2}, \\ c_1^2c_2 + c_3[c_1 + c_2(1 + \frac{d_2}{c_2})]^2 + c_1^2d_3 &= \frac{1}{3}, \\ c_1c_2c_3 &= \frac{1}{6}. \end{aligned}$$

There are two parameter families of solutions to the preceding set of equations. The scheme will be self–starting if $d_1 = 0$. One parameter families of solution to the set of equations is,

$$\begin{aligned} c_1 &= 8/15, & d_1 &= 0 \\ c_2 &= 5/12, & d_2 &= -17/60 \\ c_3 &= 3/4, & d_3 &= -5/12 \end{aligned}$$

A test case is performed to verify the order of accuracy for the time advancement scheme. The equation

$$\frac{du}{dt} = -u(t) \tag{13}$$

has an exact solution of $u(t) = e^{-t}$ when the initial condition is set to $u(0) = 1$. Hence, the right hand side of Eq. (13) and the initial condition $u(0) = 1$ are used to solve for $u(t)$ at $t = 1$ using different time increments. The maximum errors between the numerical results and the exact solution are shown in Fig. 4 which clearly indicates that the order of accuracy is approximately three.

8. CODE VERIFICATION

The accuracy of the results are verified using an exact solution of the governing equation. $T(r,t) = 300 + t + 4\alpha r^2$ is used as the solution of Eq. 2 with $\alpha = \frac{1}{4}$. This can be used as a means of verification providing that the boundary condition and initial condition are prepared using the exact solution. The results at any time level of the simulation can be assessed. The application of null derivative boundary condition can also be verified by taking the rate of temperature distribution at ($r = 0$). Figure 7 shows the temperature distribution at different time levels. The distribution corresponds to $t = 0$. is used as an initial condition in inverse simulation. Boundary condition at $r = 0$ is shown in Figure 5 which relates to the first line. Since the difference between the first two lines of this graph can not be distinguished, the application of null derivative boundary condition is assessed. Solution of the heat conduction problem in direct manner needs the specification of boundary condition at ($r = R$), which is temperature time history, and initial condition at $t = T$, which is temperature distribution. Taking the obtained temperature time trace and temperature distribution just obtained one can solve heat conduction problem in direct manner and check the temperature time trace at rod center. The simulation in this way needs negative value for the time increment and the same time step as we use in inverse modeling. Temperature distribution obtained to be exactly the same as shown by figure 6. Temperature time history obtained is the same as illustrated by figure 5.

9. EXPERIMENTAL RESULTS

An experimental data measured at the rod center of a steel slab is used to predict the surface rod temperature and oven room temperature. The data, shown in figure 8, represents the boundary condition which is regarded as time temperature trace. Since the time increment in the data file is different from the time increment needs by numerical simulation, data are interpolated by linear interpolation. In the inverse part of the numerical simulation the time trace at the rod surface and the oven temperature are calculated and

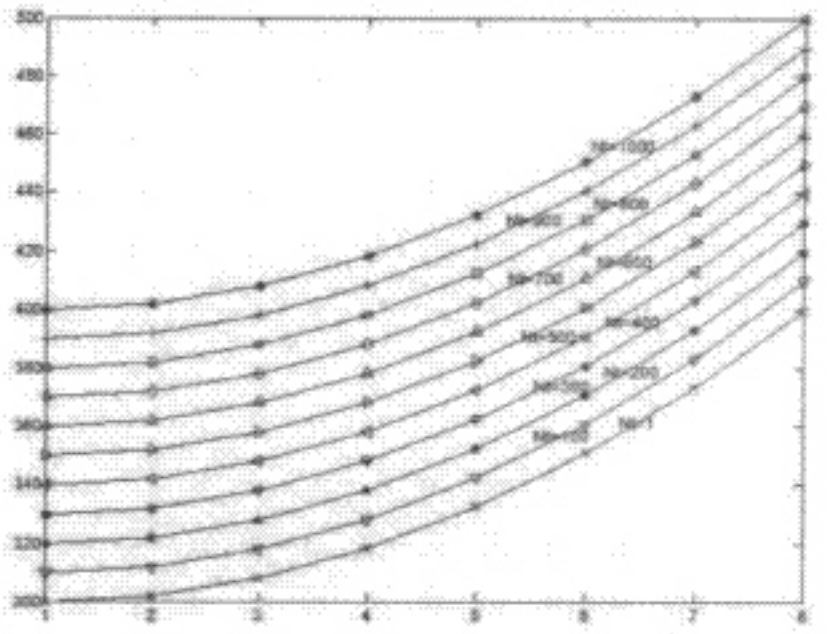

Figure 6: Temperature distribution in direct heat conduction simulation for the test case of $T(r,t) = 300 + t + 4\alpha r^2$

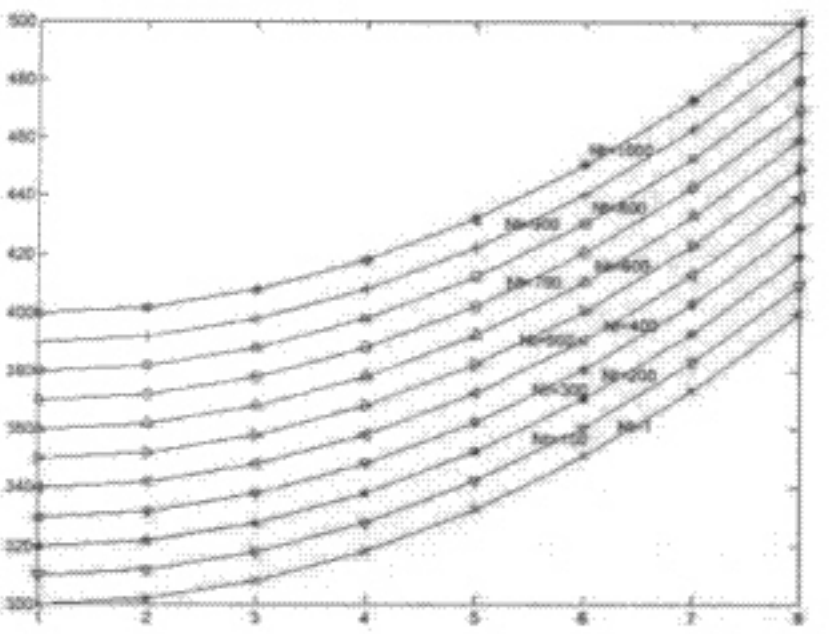

Figure 7: Temperature distribution in inverse heat conduction simulation for the test case of $T(r,t) = 300 + t + 4\alpha r^2$

shown in the figure as the middle and top curve. Temperature distributions in the rod at different time levels are shown in figure 9. Even through the use of experimental data any inverse problem can be verified. Taking the last distribution as an initial condition in the direct approach and using the temperature time trace at the the rod surface as the boundary condition a direct approach can be applied and the temperature time trace at $r = 0$ is justified against the boundary condition of inverse approach. The results shows that the inverse and direct modeling of heat conduction problem are performed appropriately and the proposed approach of implementing the numerical model can be extend to the cases where the change in thermal diffusivity is ignored.

10. CONCLUSIONS

Numerical Simulation of inverse heat conduction problem is conducted in one dimensional polar coordinate system. This simulation is performed in order to properly determine the boundary condition required for obtaining a specific property of a metal under the heat treatment operation in an oven. The boundary condition which is proposed by the inverse method is found to be appropriate for producing the desirable metal property. Therefore, in this study the oven condition which produce a known metal properties is obtained. The condition is then used for the heat treatment of a metal contained in an oven. This condition can be controlled in areal practice. The simulation shows the power of numerical modeling to determine exact applicable conditions for the heat treatment of a specimen in an oven. The traditional method uses the trial and error approach which is very time consuming and cost-demanding. The spatial derivatives of this simulation are calculated using a compact finite difference scheme. The time advancement of the simulation is performed using the compact third order Runge–Kutta scheme. The determined boundary condition is then used in the direct numerical simulation of time dependant heat conduction. This is performed to check the accuracy of the inverse solution. The results indicates that the method is quite efficient in determining a proper boundary condition for the rod surface.

11. REFERENCES

[1] Reti T., Gergely, M., "Computerized Process Planning in Heat-Treatment Practice Using Personal Computers" , HEAT TREATMENT OF METALS, 1991, Vol 18, Iss 4, pp 117-121

[2] Umemoto M., Hiramatsu A., Moriya A., Watanabe T. Nanba S., Nakajima N., Anan G. and Higo Y., "Computer Modeling of Phase-Transformation from Work-Hardened Austenite", ISIJ INTERNATIONAL ,1992, Vol 32, Iss 3, pp 306-315

[3] Suehiro-M Senuma-T Yada-H Sato-K, " Application of Mathematical-Model for Predicting Microstructural Evolution to High-Carbon Steels", ISIJ INTERNATIONAL, 1992, Vol 32, Iss 3, pp 433-439

[4] Kwon O., "A Technology for the Prediction and Control of Microstructural Changes and Mechanical-Properties in Steel" ,ISIJ INTERNATIONAL ,1992, Vol 32, Iss 3, pp 350-358

[5] Kurpisz-K Nowak-AJ, "BEM Approach to Inverse Heat-Conduction Problems", ENGINEERING ANALYSIS WITH BOUNDARY ELEMENTS, 1992, Vol 10, Iss 4, pp 291-297

[6] S. K. Lele., "Compact Finite Difference Schemes with Spectral–Like Resolution", J. Comp. Phys., Vol 103, pp 16–42, 1992.

[7] M.J. Maghrebi., "A Study of the Evolution of Intense Focal Structures in Spatiallt Developing Three–Dimensional Plane Wakes", PhD Thesis, Monash University, 1999.

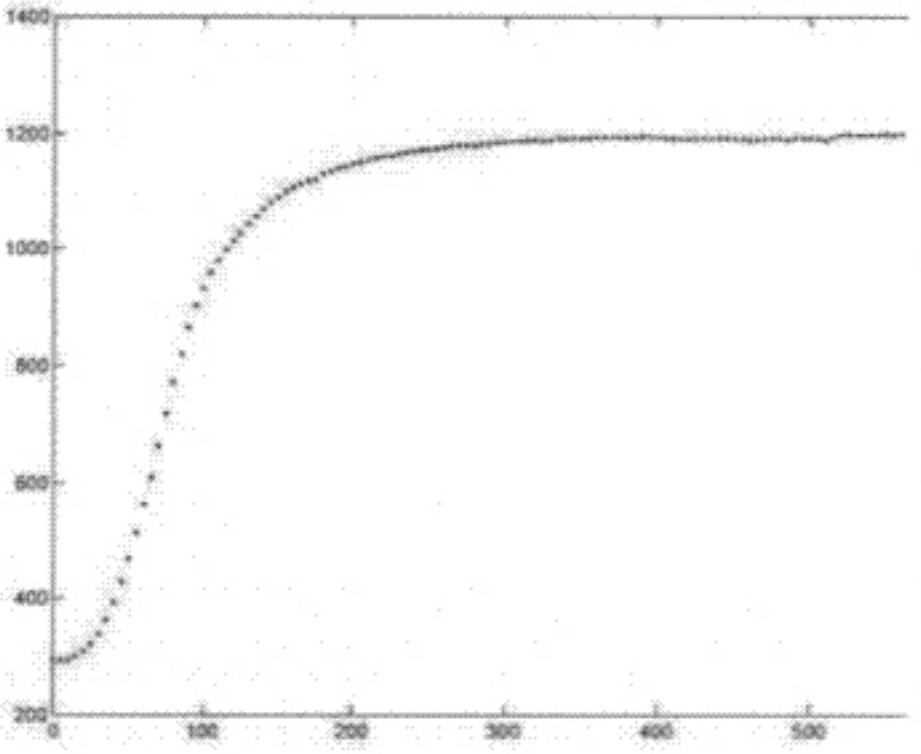

Figure 8: Experimental data for temperature time trace at the steel rod center

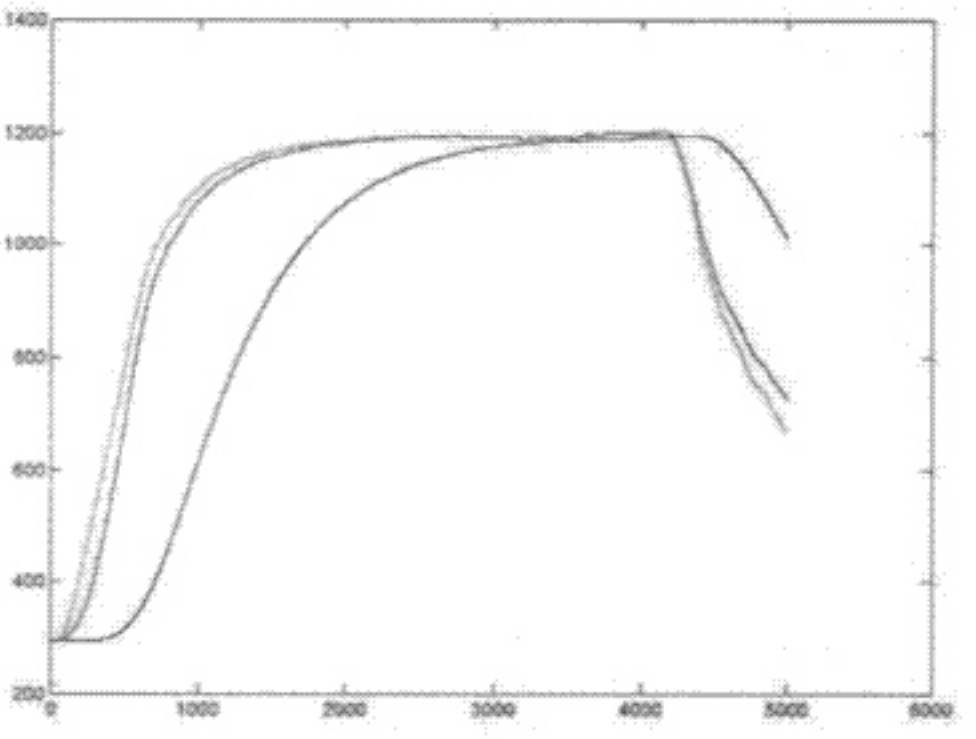

Figure 10: Temperature–time trace and oven temperature history in both inverse and direct heat conduction simulation of a steel rod.

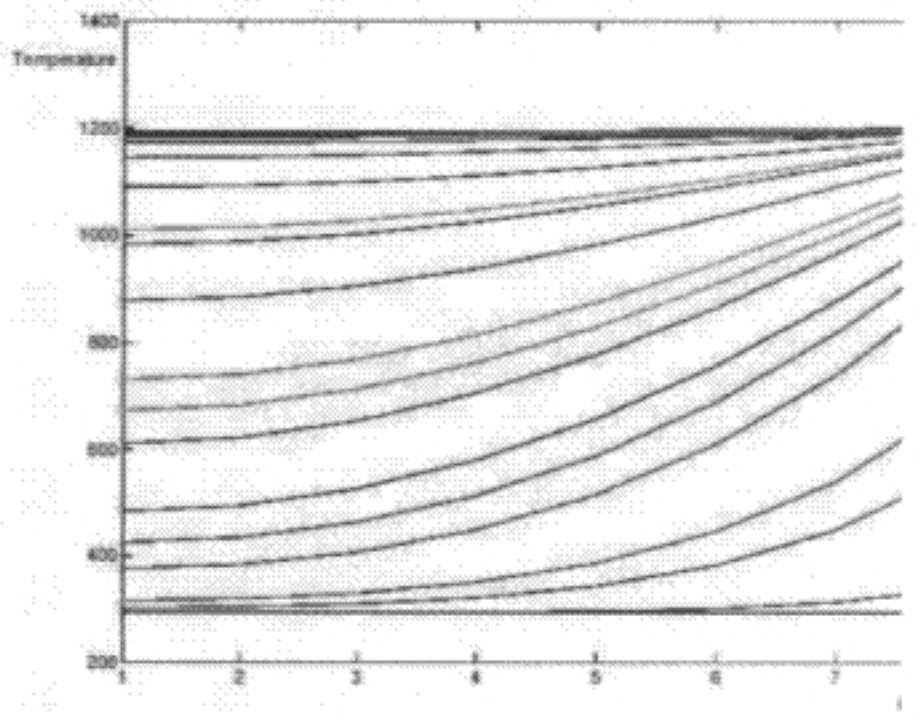

Figure 9: Temperature distribution of inverse heat conduction simulation for a steel rod

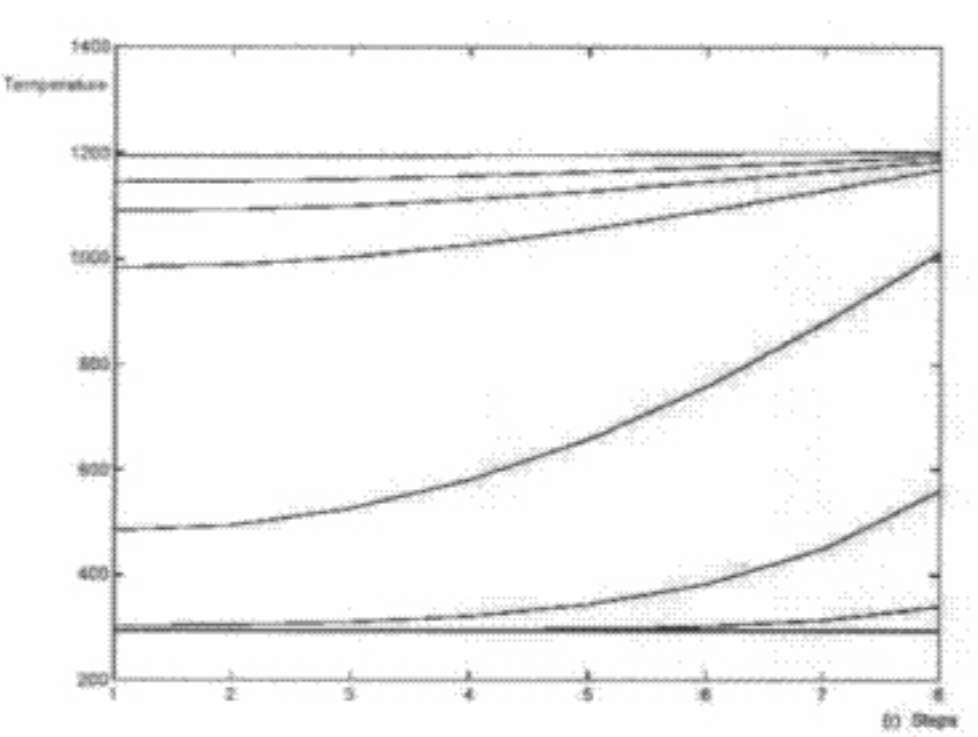

Figure 11: Temperature distribution of direct heat conduction simulation for a steel rod